Optics Letters

Bloch oscillations in photonic spectral lattices through phase-mismatched four-wave mixing

Wenwan Li,[1] Chengzhi Qin,[1,4] Tianwen Han,[1] Hao Chen,[1] Bing Wang,[1,*] and Peixiang Lu[1,2,3]

[1]Wuhan National Laboratory for Optoelectronics and School of Physics, Huazhong University of Science and Technology, Wuhan 430074, China
[2]Hubei Key laboratory of Optical Information and Pattern Recognition, Wuhan Institute of Technology, Wuhan 430205, China
[3]e-mail: lupeixiang@hust.edu.cn
[4]e-mail: qinchengzhi@hust.edu.cn
*Corresponding author: wangbing@hust.edu.cn

Received 11 September 2019; revised 8 October 2019; accepted 11 October 2019; posted 14 October 2019 (Doc. ID 377086); published 6 November 2019

Here we investigate the Bloch oscillations (BOs) in a photonic spectral lattice created with four-wave mixing Bragg scattering (FWM-BS). By injecting a signal and two pumps with different frequencies into a silicon nitride waveguide, a spectral lattice can be created for the generated idlers through successive FWM-BS. The phase-mismatch during FWM-BS acts as an effective force that induces BOs in the spectral lattice. Both the oscillation period and amplitude are determined by the magnitude of the effective force. With cascaded FWM-BS processes, the spectrum of idlers experiences a directional shift as the phase differences of pumps are modulated. Additionally, introducing long-range couplings in the spectral lattice will change the trajectory of BOs within each period. The pattern of BOs for a single frequency input can also be tailored. This Letter provides a new platform to realize BOs in the frequency dimension and paves a promising way for broadband frequency control with all-optical schemes.

https://doi.org/10.1364/OL.44.005430

As imposed by a constant electric force, electrons in a crystal lattice will manifest periodic oscillation motions. The effect is known as Bloch oscillations (BOs), which have been experimentally observed in many solid systems [1,2]. Apart from electrons, photons can also take on BOs in discrete optical systems, such as curved waveguide arrays and optical lattices with gradient potentials [3–6]. Recently, BOs have been demonstrated in frequency dimension by detecting the evolution of a light spectrum in dynamically modulated optical waveguides and resonators [7,8]. However, the dynamic modulation implemented by electro-optic modulators is subject to the intrinsic limited bandwidth in gigahertz range [7–12]. To fulfill a larger bandwidth requirement in optical communication and signal processing [13], recent efforts have been dedicated to all-optical techniques based on nonlinear optical processes [14–16], of which the four-wave mixing Bragg scattering (FWM-BS) has been utilized to create spectral lattice for controlling photons [14,17–19]. Compared with electro-optic modulation, the FWM-BS process manifests lower loss and larger bandwidth up to terahertz, resulting in more efficient manipulation of a light spectrum.

In FWM-BS, the phase-match condition is usually required to achieve high conversion efficiency. Here we find that a slight phase-mismatch can induce an effective force for photons and arouse BOs of the generated idler in the frequency dimension. By cascading multiple FWM-BS processes and modulating the phases of pumps, the directional shift of a light spectrum can be achieved. Additionally, anharmonic Bloch oscillations (ABOs) in frequency dimension are also observed by introducing more pumps in the FWM-BS process [20]. This Letter provides a unique platform to demonstrate BOs in frequency dimension and may find applications in all-optical frequency control.

The FWM-BS is implemented in a strip waveguide with a core of Si_3N_4 [17,18] embedded in SiO_2. The dimensions of the cross section of the core are 700 nm × 300 nm, as shown in Fig. 1(a). A signal with frequency ω_s and two pumps with frequencies $\omega_{p1,2}$ are incident together into the waveguide. They are all continuous waves and can be generated by a mode-locked laser [14]. The profile of fundamental TE_0 mode in the waveguide is shown in the inset. The field is mainly concentrated in the core region. As a signal photon is scattered by two pump photons, the idler photons are generated at frequencies $\omega_i = \omega_s \pm \Omega$ [19]. When the phase-match condition is satisfied, the successive FWM-BS processes will occur, giving rise to a spectral lattice $\omega_n = \omega_s + n\Omega$ $(n = 0, \pm 1, \pm 2, \ldots)$, as shown in Fig. 1(b). The lattice constant $\Omega = \omega_{p2} - \omega_{p1}$ is uniquely determined by the frequency interval between the two pumps. The total field in the waveguide can be written as [21]

$$U = \sum_{n=-\infty}^{\infty} a_n(z) e^{i(\beta_n z - \omega_n t)} + A_1(z) e^{i(\beta_{p1} z - \omega_{p1} t + \phi_1)} + A_2(z) e^{i(\beta_{p2} z - \omega_{p2} t + \phi_2)}, \quad (1)$$

where $a_n(z)$ and β_n are the amplitude and propagation constant, respectively, of the idler at frequency ω_n. The frequency of input signal equals ω_0. $A_{1,2}(z)$ represent the amplitudes of the two pumps. The propagation constants and initial phases of the pumps are denoted by $\beta_{p1,p2}$ and $\phi_{1,2}$, respectively.

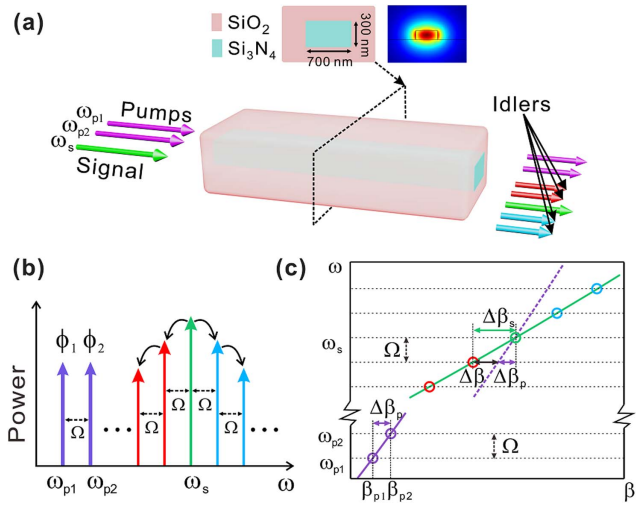

Fig. 1. (a) Schematic diagram of FWM-BS in the Si_3N_4 waveguide. The insets show the cross section and fundamental TE_0 mode of the waveguide. (b) Synthetic spectral lattice created by FWM-BS. Ω is the frequency interval of generated idlers. ϕ_1 and ϕ_2 are the initial phases of the input pumps with frequencies ω_{p1} and ω_{p2}, respectively. ω_s denotes the frequency of signal. (c) Dispersion relation of fundamental modes in the Si_3N_4 waveguide. The green and purple lines indicate the dispersion relation near the pump and signal frequencies. $\Delta\beta_s$ and $\Delta\beta_p$ are the wavevector interval of adjacent idlers and that of pumps. The wavevector mismatch of FWM-BS is denoted by $\Delta\beta$.

The dispersion relations of the pumps and idlers are shown in Fig. 1(c). They are treated as fundamental modes with different frequencies in the waveguide. Due to the dispersion of Si_3N_4, the group velocities of the modes in distinct frequencies are different. Considering that $\Omega \ll \omega_s$, the dispersion curve for the idlers near ω_s, as well as for the pumps near ω_{p1} and ω_{p2}, can be treated as a straight line. Hence, the wavevector mismatch is given by

$$-\Delta\beta = (\beta_{p1} - \beta_{p2}) - (\beta_{n+1} - \beta_n). \tag{2}$$

The FWM-BS process is governed by the nonlinear Schrödinger equation [21]

$$\frac{\partial U}{\partial z} = i\gamma|U|^2 U, \tag{3}$$

where γ is nonlinear coefficient of the Si_3N_4 waveguide. Using the undepleted pump approximation in which the pump amplitudes are treated as constants, and substituting Eq. (1) into Eq. (3), we could obtain the coupled-mode equation for the idlers:

$$\frac{\partial a_n(z)}{\partial z} = iC[a_{n-1}(z)e^{i(-\Delta\beta z+\Delta\phi)} + a_{n+1}(z)e^{-i(-\Delta\beta z+\Delta\phi)}], \tag{4}$$

where $C = 2\gamma A_1(0)A_2(0)$ is the coupling strength between adjacent modes, and $\Delta\phi = \phi_1 - \phi_2$ denotes the phase difference between the two pumps.

First, we consider the eigen Bloch mode in the spectral lattice, i.e., an infinite-width frequency comb $a_n(z) = a_0 \exp(in\phi_0)\exp(ik_z z)$, where a_0 is the amplitude, and $\phi_0 = k_\omega(0)\Omega$ and k_z are the initial Bloch momentum in the frequency dimension and propagation constant, respectively, along the waveguide. Substituting $a_n(z)$ into Eq. (4) and assuming $z dk_z/dz \ll k_z$, we can obtain the band structure for the spectral lattice:

$$k_z[\phi_\omega(z)] = 2C\cos[\phi_\omega(z) - \Delta\phi], \tag{5}$$

where $\phi_\omega(z) = \phi_0 + \Delta\beta z$, denoting a linearly varying Bloch momentum during propagation. Thus, a constant effective force $F = \partial\phi_\omega(z)/\partial z = \Delta\beta$ is generated in the spectral lattice. Figure 2(a) shows the band structures for $\Delta\phi = 0$ and π. Denoting $\phi_\omega(z) = k_\omega(z)\Omega$ and considering a finite-width frequency comb input into the waveguide, the group velocity in spectral lattice is given by $v_g(z) = -\partial k_z[k_\omega(z)]/\partial k_\omega(z) = 2C\Omega\sin(\phi_0 + \Delta\beta z - \Delta\phi)$, which is perpendicular to the band structure. Thus, the accumulated spectral shift is obtained by

$$\omega(z) = -\frac{2C\Omega}{\Delta\beta}[\cos(\phi_0 + \Delta\beta z - \Delta\phi) - \cos(\phi_0 - \Delta\phi)]. \tag{6}$$

It appears that the center-of-mass of the frequency comb manifests a cosine oscillatory motion in the spectral lattice, which refers exactly to BOs in the frequency dimension. The corresponding oscillation period is

$$T_{\mathrm{BO}} = \frac{2\pi}{\Delta\beta}, \tag{7}$$

which is inversely proportional to the mismatched wavevector.

The theoretical analysis above can be verified by the numerical simulations of spectrum evolutions of idler lights in the waveguide. The wavelengths of the pumps are $\lambda_{p1} = 1550$ nm and $\lambda_{p2} = 1550.4$ nm; the wavelength of the signal $\lambda_s = 1330$ nm. The corresponding frequency difference of the pumps is $\Omega/2\pi = 50$ GHz. The peak powers of the pumps have the same value of 15 W [17]. According to the above parameters, we can obtain the wavevector mismatch $-\Delta\beta = -0.0001\ \mu\mathrm{m}^{-1}$ and, hence, $T_{\mathrm{BO}} = 2\pi/\Delta\beta = 62.8$ mm. In order to observe BOs, we choose the length of the waveguide

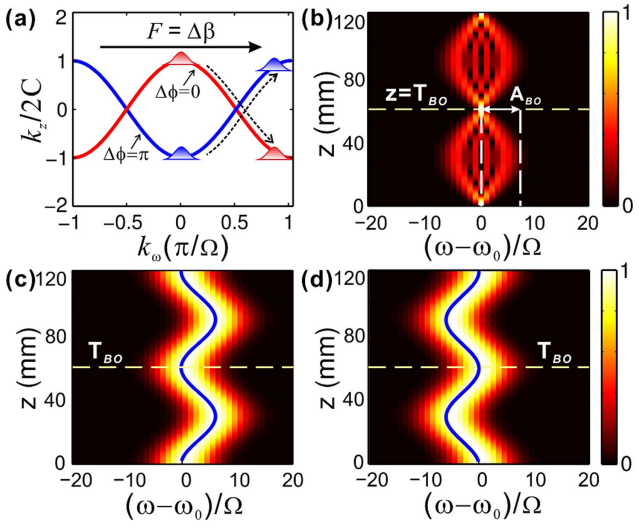

Fig. 2. (a) Band structures of the spectral lattice for $\Delta\phi = 0$ (red) and $\Delta\phi = \pi$ (blue). $F = \Delta\beta$ denotes the effective force, which makes the Bloch momentum shift over the band curve along the dashed line. (b) Spectral evolution of BOs for a single frequency input. T_{BO} and A_{BO} are the period and amplitude of BOs, respectively. (c), (d) Spectral evolutions of BOs under a Bloch wave packet input for (c) $\Delta\phi = 0$ and (d) $\Delta\phi = \pi$. The dashed lines denote $z = T_{\mathrm{BO}}$, and the blue curves represent the theoretical predictions of oscillation trajectories.

as 126 mm [22]. Additionally, the effect of dispersion on the spectrum evolution is negligible due to the dispersion curve being almost linear in the vicinity of frequencies of the signal and idler lights. The results obtained by numerically solving Eq. (4) are illustrated in Figs. 2(b)–2(d). Almost the same results can be achieved by solving Eq. (3) using the split-step Fourier method [14], as the power of the pumps is much larger than that of the signal. Figure 2(b) shows the spectrum evolution of idlers with a single frequency input. The spectrum experiences a periodically breathing behavior during propagation, and a self-focusing effect appears repeatedly with a period of 63 mm, which coincides fairly with the theoretical prediction of T_{BO}. We also input a Bloch wave packet, which is obtained by truncating a frequency comb into a finite-width $W = 5\Omega$. As the initial Bloch momentum of the wave packet $\phi_0 = 0$, that is, the incident modes in the packet are all in phase, the spectrum evolution of generated idlers is shown in Fig. 2(c) for $\Delta\phi = 0$. The trajectory of the spectrum center follows a cosine function, which agrees well with the theoretical prediction depicted by the blue curve. The effect of BOs can be explained by the band structure shown in Fig. 2(a). Due to the effective force, the Bloch momentum of idlers should experience a continuous shift along to the right, and the group velocity changes periodically according to the shape of the band curve. Consequently, the spectrum undergoes a periodic oscillation. For $\Delta\phi = \pi$, the group velocity at the same Bloch momentum is opposite in lateral direction to that for the case $\Delta\phi = 0$. The BOs show an opposite phase in contrast to the latter, as shown in Fig. 2(d). In both cases, the amplitude of the BOs $A_{\mathrm{BO}} = 2\pi \times 287$ GHz, which also agrees well with the theoretical value.

Since BOs are periodically oscillatory motions, as demonstrated above, the maximum spectral shift is limited by the finite oscillation amplitude. Nevertheless, by cascading multiple processes of FWM-BS with different $\Delta\phi$ for the pumps, the periodic nature of BOs might be broken, and aperiodic spectral shifting can be achieved. The phase difference $\Delta\phi$ of the pumps in each process can be varied by the optical delay line (ODL), as shown in Fig. 3(a). Here we depict two segments of waveguides as an example. After each waveguide, the pumps are filtered out, and the generated idlers are combined with pumps which are phase delayed through another route. Without loss of generality, we numerically simulate the spectral evolution in the case of directly cascading four segments of Si_3N_4 waveguides, each of which has a fixed length of $L = 0.5T_{\mathrm{BO}}$. The phase differences in each segment are $\Delta\phi = 0$, π, 0, and π. Figures 3(b)–3(d) show the spectral evolutions for the incidence of a Bloch wave packet. Here all parameters are the same as that in Fig. 2. As the Bloch wave packet carries an initial Bloch momentum $\phi_0 = 0$, it experiences a directional spectral blueshift, as shown in Fig. 3(b). While for $\phi_0 = \pi$, as shown in Fig. 3(c), the Bloch wave packet undergoes a directional spectral redshift, which manifests a mirror symmetry with respect to that in Fig. 3(b). Both the accumulated spectral blueshift and redshift reach $|\Delta\omega| = 4A_{\mathrm{BO}} = 16C\Omega/\Delta\beta$. If we choose $\phi_0 = \pi/2$, as illustrated in Fig. 3(d), the spectral directional shift does not occur, and the wave packet exhibits a periodic localization with the envelope center recovering to the initial position at the end of each segment. Finally, we consider the spectral evolution under a single frequency input into the system, as shown in Fig. 3(e). Differing from the periodically self-focusing pattern, as obtained in Fig. 2(b), the single frequency

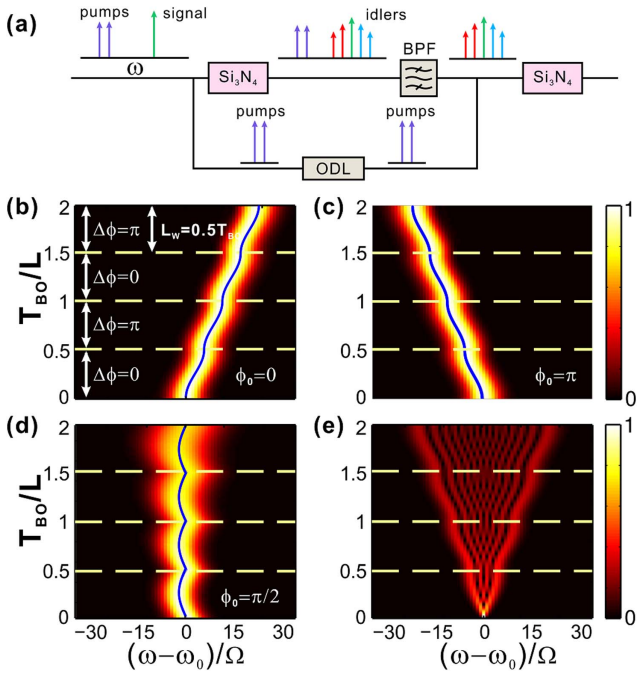

Fig. 3. (a) Schematic diagram for cascading multiple FWM-BS processes. ODL, optical delay line; BPF, bandpass filter. (b), (c), and (d) Spectrum evolutions of four cascaded processes of FWM-BS for the Bloch wave packet input with initial Bloch momentum (b) $\phi_0 = 0$, (c) $\phi_0 = \pi$, and (d) $\phi_0 = \pi/2$. (e) Spectrum evolution for a single frequency input. The yellow dashed lines indicate the interfaces of different waveguides. The blue curves denote the theoretical trajectories.

exhibits successive discrete diffraction and bandwidth expansion, with the bandwidth reaching $8A_{\mathrm{BO}} = 32C\Omega/\Delta\beta$ which will be greater than terahertz at the output.

In the above discussion, BOs are formed by the nearest-neighbor coupling, where only two pumps are involved in the FWM-BS. However, by introducing a third pump into the process, the long-range coupling can be realized, giving rise to ABOs in frequency dimension [7,18]. Assuming the frequency interval between the second and third pumps is 2Ω, the coupled-mode equation for the idler lights can be written as the superposition of three sets of BOs, which reads

$$\frac{\partial a_n(z)}{\partial z} = i\sum_{m=1}^{3}[C_m(a_{n-m}(z)e^{i(-m\Delta\beta z+\Delta\phi_m)} + a_{n+m}(z)e^{-i(-m\Delta\beta z+\Delta\phi_m)})], \tag{8}$$

where $C_1 = 2\gamma A_1(0)A_2(0)$, $C_2 = 2\gamma A_2(0)A_3(0)$, and $C_3 = 2\gamma A_1(0)A_3(0)$ are coupling strengths for different order coupling. $\Delta\phi_1 = \phi_1 - \phi_2$, $\Delta\phi_2 = \phi_2 - \phi_3$, and $\Delta\phi_3 = \phi_1 - \phi_3$ are the phase differences between different pumps. Considering an infinite-width frequency comb input, the band structure can be expressed as

$$k_z(\phi_\omega(z)) = 2\sum_{m=1}^{3} C_m \cos(\phi_0 + \Delta\beta z - \Delta\phi_m), \tag{9}$$

and we can obtain the accumulated spectral shift

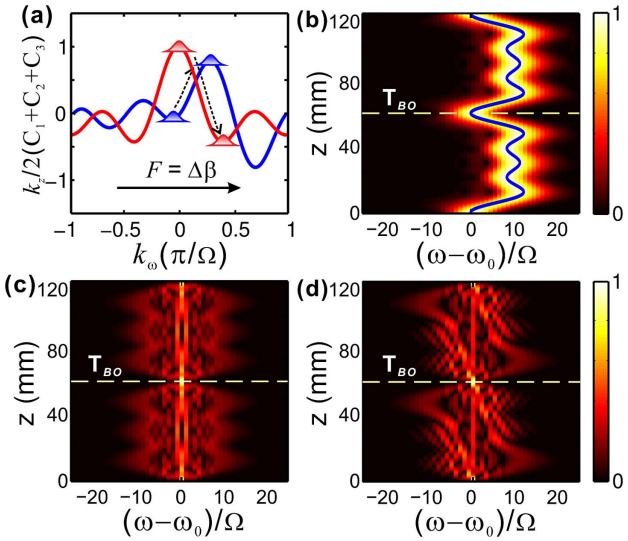

Fig. 4. (a) Band structures in the spectral lattice for $\Delta\phi_1 = \Delta\phi_2 = \Delta\phi_3 = 0$ (red) and $\Delta\phi_1 = 0$, $\Delta\phi_2 = \pi/2$, and $\Delta\phi_3 = \pi$ (blue). The Bloch momentum shifts under the effective force $F = \Delta\beta$. The dashed line denotes the shift direction. (b) Spectrum evolution of ABOs for a Bloch wave packet input. The blue solid curve denotes the theoretical result. (c), (d) Spectral oscillation patterns of ABOs for a single frequency input by choosing (c) red and (d) blue band structures. The yellow dashed lines denote the position $z = T_{\mathrm{BO}}$.

$$\omega(z) = -\sum_{m=1}^{3} \frac{2C_m\Omega}{\Delta\beta}[\cos(\phi_0 + \Delta\beta z - \Delta\phi_m) - \cos(\phi_0 - \Delta\phi_m)]. \tag{10}$$

Figure 4(a) shows the band structures in the presence of long-range coupling. As $C_1 = C_2 = C_3$ and $\Delta\phi_1 = \Delta\phi_2 = \Delta\phi_3 = 0$, the band structure has a symmetric shape, as depicted by the red curve in the figure. The spectral evolution under an input of Bloch wave packet is shown in Fig. 4(b). Since the band structure and spectrum shift follow the same function, as shown in Eqs. (9) and (10), the oscillation trajectory is analogous to the shape of the band structure. Apart from controlling the oscillation trajectory, the pattern of the spectrum evolution can also be controlled by tailoring the band curve. For example, we construct an asymmetric band structure, as depicted by the blue curve in Fig. 4(a) for $C_1 = C_2 = C_3$ and $\Delta\phi_1 = 0$, $\Delta\phi_2 = \pi/2$, and $\Delta\phi_3 = \pi$. The spectrum evolutions for a single frequency input of signal are shown in Figs. 4(c) and 4(d), as the band curves are symmetric and asymmetric. The breathing oscillation patterns show distinct symmetry according to the band structure. The symmetry of the oscillation pattern is attributed to the time-reversal symmetry (TRS) of the band structure [9]. The input of single frequency arouses arbitrary Bloch momentums all over the Brillouin zone. As the band structure manifests TRS, i.e., $k_z(k_\omega) = k_z(-k_\omega)$, any opposite Bloch-mode components at k_ω and $-k_\omega$ contribute equally to the spectrum evolution, resulting in a symmetric pattern of BOs, as shown in Fig. 4(c). On the other hand, as the TRS is broken, the oscillation pattern becomes asymmetric, as shown in Fig. 4(d).

In summary, we have studied BOs in a synthetic spectral lattice created by successive FWM-BS processes in the Si_3N_4 waveguides. By choosing different frequency regions of the signal and pumps, a slight wavevector mismatch can be achieved due to the waveguide dispersion. Thus, an effective force is introduced in the spectral lattice, and the spectrum of generated idlers undergoes BOs. By cascading multiple FWM-BS processes with distinct phase differences between adjacent pumps, the spectrum of BOs is no longer periodic, and aperiodic spectral shifting appears. By introducing long-range couplings in the spectral lattice with more pumps, the ABOs can also be achieved. For an input of single frequency, the breathing oscillation patterns of BOs can be symmetric and asymmetric by tailoring the band structure of the Bloch modes in the spectral lattice. This Letter paves a promising way towards all-optical manipulation of a light spectrum and may find many applications in optical communication and signal processing, such as temporal-spectral imaging and information reconstruction [23,24].

Funding. National Natural Science Foundation of China (11674117, 11974124); National Postdoctoral Program for Innovative Talents (BX20190129).

Disclosures. The authors declare no conflicts of interest.

REFERENCES

1. C. Waschke, H. G. Roskos, R. Schwedler, K. Leo, H. Kurz, and K. Köhler, Phys. Rev. Lett. **70**, 3319 (1993).
2. S. R. Wilkinson, C. F. Bharucha, K. W. Madison, Q. Niu, and M. G. Raizen, Phys. Rev. Lett. **76**, 4512 (1996).
3. T. Pertsch, P. Dannberg, and W. Elflein, Phys. Rev. Lett. **83**, 4752 (1999).
4. S. Longhi, Opt. Lett. **30**, 2137 (2005).
5. F. Xiao, B. Li, M. Wang, W. Zhu, P. Zhang, S. Liu, M. Premaraten, and J. Zhao, Opt. Express **22**, 22763 (2014).
6. U. Peschel, T. Pertsch, and F. Lederer, Opt. Lett. **23**, 1701 (1998).
7. C. Qin, L. Yuan, B. Wang, S. Fan, and P. Lu, Phys. Rev. A **97**, 063838 (2018).
8. L. Yuan and S. Fan, Optica **3**, 1014 (2016).
9. C. Qin, F. Zhou, Y. Peng, D. Sounas, X. Zhu, B. Wang, J. Dong, X. Zhang, A. Alù, and P. Lu, Phys. Rev. Lett. **120**, 133901 (2018).
10. L. Yuan, Q. Lin, M. Xiao, and S. Fan, Optica **5**, 1396 (2018).
11. L. Ding, C. Qin, F. Zhou, L. Yang, W. Li, F. Luo, J. Dong, B. Wang, and P. Lu, Phys. Rev. Appl. **12**, 024027 (2019).
12. H. Chen, C. Qin, B. Wang, and P. Lu, Opt. Lett. **44**, 363 (2019).
13. L. Fan, C. Zou, M. Poot, R. Cheng, X. Guo, X. Han, and H. Tang, Nat. Photonics **10**, 766 (2016).
14. B. A. Bell, K. Wang, A. S. Solntsev, D. N. Neshev, A. A. Sukhorukov, and B. J. Eggleton, Optica **4**, 1433 (2017).
15. D. J. Moss, R. Morandotti, A. L. Gaeta, and M. Lipson, Nat. Photonics **7**, 597 (2013).
16. D. M. Kinyua, L. Niu, H. Long, K. Wang, and B. Wang, Opt. Mater. **96**, 109311 (2019).
17. I. Agha, M. Davanço, and B. Thurston, Opt. Lett. **37**, 2997 (2012).
18. Q. Li, M. Davanço, and K. Srinivasan, Nat. Photonics **10**, 406 (2016).
19. K. Li, H. Sun, and A. C. Foster, Opt. Lett. **42**, 1488 (2017).
20. F. Dreisow, G. Wang, and M. Heinrich, Opt. Lett. **36**, 3963 (2011).
21. G. P. Agrawal, *Nonlinear Fiber Optics* (Academic, 2001).
22. C. J. Krückel, V. Torres-Company, P. A. Andrekson, D. T. Spencer, J. F. Bauters, M. J. R. Heck, and J. E. Bowers, Opt. Lett. **40**, 875 (2015).
23. C. Bersch, G. Onishchukov, and U. Peschel, Opt. Lett. **34**, 2372 (2009).
24. C. Bersch, G. Onishchukov, and U. Peschel, Appl. Phys. B **104**, 495 (2011).